Supporting information materials for

On the Flexibility of Metal-Organic Frameworks

Lev Sarkisov[1,*], Richard L. Martin[2], Maciej Haranczyk[2], Berend Smit[3,4,*]

[1]Institute for Materials and Processes, School of Engineering, The University of Edinburgh, Edinburgh, EH9 3JL, United Kingdom.

[2]Computational Research Division, Lawrence Berkeley National Laboratory, One Cyclotron Road, Mail Stop 50F-1650, Berkeley, California 94720-8139, United States.

[3]Department of Chemical and Biomolecular Engineering, University of California, Berkeley, California 94720, United States.

[4]Materials Sciences Division, Lawrence Berkeley National Laboratory, Berkeley, California 94720-8139, United States.

*Correspondence to: Lev.Sarkisov@ed.ac.uk; Berend-Smit@berkeley.edu

Supporting Materials:

Figures S1-S14

Tables S1-S6

Movies and visualizations: http://www.nanoporousmaterials.org/flexibility/

References (1-16)

Table of Contents

Section S1. Construction of representation of MOFs as systems of molecular trusses

Here we provide a detailed explanation of the principles for the construction of a truss representation of a MOF. For this we use IRMOF-1 as an example. In Fig. S1 (A), we show the molecular structure of IRMOF-1. The constituent elements, metal-oxygen secondary building units (SBUs) and organic linkers, can be considered as rigid. Using a system of two SBUs and a linker, Fig. S1 (B) summarizes the only allowable degrees of freedom within this system. The first one is a hinge rotation of the linker element around the axis that connects two oxygen atoms, to which the linker is attached. The second one is rotation of the clusters of atoms included in the ovals with respect to each other around the axis connecting carbon atoms of the two COO groups. Here we call it axial rotation, with the axis shown as a vertical line in Fig. S1 (B).
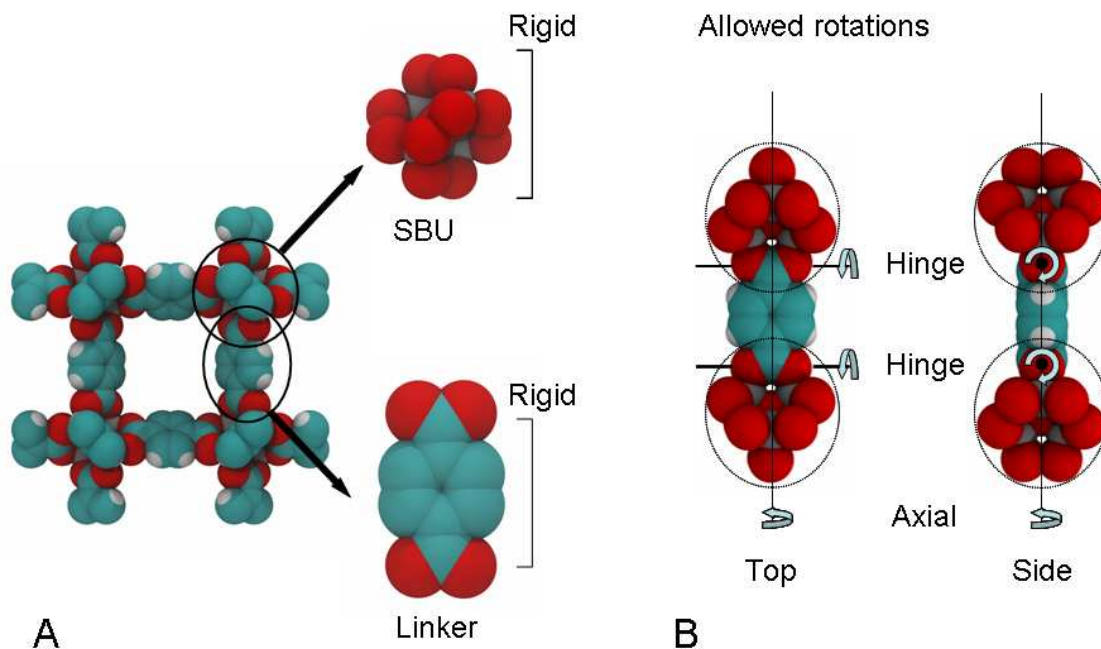

Fig. S1. (A) Molecular structure of IRMOF-1 and rigid elements it consists of. (B) Allowed degrees of freedom in the assembly of two SBUs and a linker, considered from two different perspectives (top and side).

The idea of the approach developed here is to reduce the molecular structure of a MOF to a system of molecular trusses, in such a way that it correctly reflects the rigidity of the constituent elements, SBUs and linkers, and the nature of connections and rotations between them. For this we developed a simple algorithm, which we illustrate in Fig. S2.

We start with the crystal structure of IRMOF-1 and remove all the details of the structure that are not important for the future considerations. For this, from the SBUs, we keep all the oxygen atoms linked to the metal atom. From the linker we keep only carbon atoms connected to the oxygen atoms of the SBUs, as shown in Fig. S2. In molecular trusses these atoms become size-less and mass-less points and we depict them as particles in Fig. S2 only for better visualization. For clarity we will use "oxygen sites" for the positions where oxygen atoms used to be and "carbon sites" to describe points of the graph where carbon atoms used to be. In case of IRMOF-1 only two carbon sites represent the BDC linker, and the same representation will apply to all the materials in IRMOF-1-IRMOF-16 series.

To maintain the rigidity of the SBU cluster, rigid bonds are imposed between all oxygen sites within a certain distance from each other (5Å). This creates a sufficient degree of cross-linking to maintain rigidity in the resulting system of molecular trusses. As these bonds have purely geometric meaning they can cross each other. In our calculations we focus on perturbations around equilibrium, but if one applies a large deformation such crossings can lead to unphysical situations.

Consider now the linker made of two carbon sites and complemented by four oxygen sites, to which the carbon sites are connected. Within this system of six sites, the bonds are placed between the two carbon sites, and between carbon and oxygen sites, as shown in Fig. S2. Two oxygen sites, which belong to the same SBU, have been already connected to each other during the generation of the molecular truss for the SBU, and this is also reflected in Fig. S2. This leads to two rigid flat tetrahedra (shown in yellow and purple in Fig. S2), each formed by two oxygen and two carbon sites. The tetrahedra can rotate with respect to each other along the axis connecting two carbon sites (shown as a dashed line); otherwise the linker behaves as a rigid structure under these constraints. Two rigid systems of molecular trusses

(corresponding to the SBU cluster and the linker), sharing the same edge, form a hinge connection as shown in the center of Fig. S2.
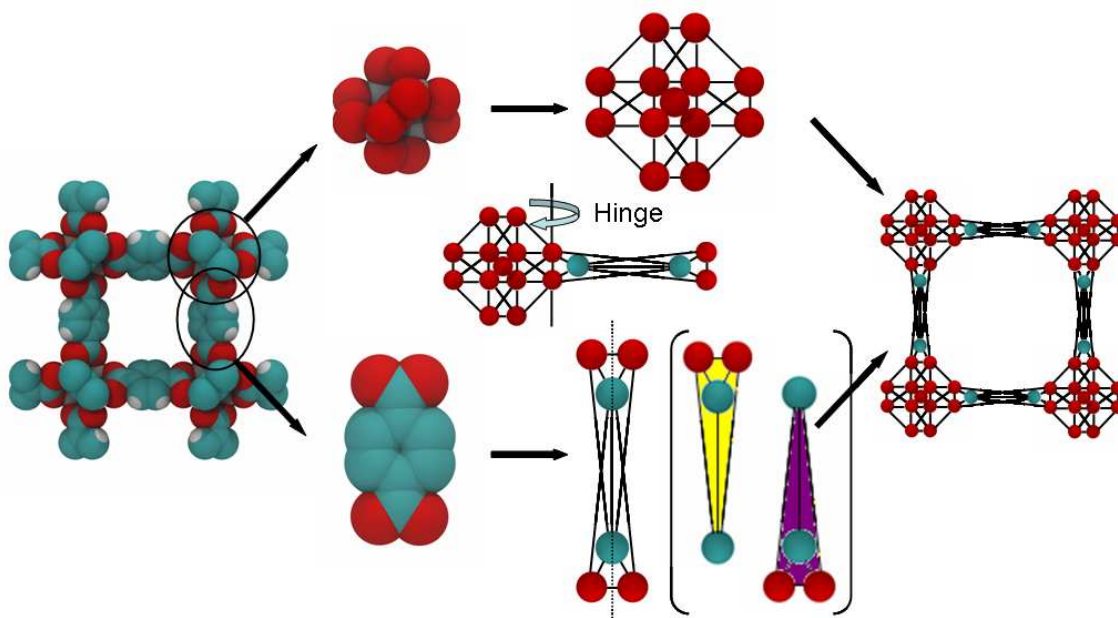

Fig. S2: Schematic illustration of the algorithm for generation of a system of molecular trusses for IRMOF-1. Within the molecular truss representation, each element is a system of points, or sites (shown as particles for convenience) connected by rigid bonds (shown as black lines). Top part of the figure shows the process for the metal-oxygen SBU (not all bonds are shown for clarity). Bottom part of the figure shows the same process for the BDC linker. The linker molecular truss consists of two tetrahedra, shown in brackets in yellow and purple, which can rotate with respect to each other around an axis passing through the carbon sites (shown as a dashed line). The linker and the SBU share two oxygen sites, forming a hinge connection, as shown in the center of the figure. The final molecular truss representation of IRMOF-1 is shown in on the right. Color scheme for the molecular visualization of IRMOF-1 on the left: cyan for carbon, red for oxygen, grey for zinc, white for hydrogen.

The truss generation algorithm can be generalized and extended to other systems. Specifically, Fig. S3 shows the same process for HKUST-1, or CuBTC. It is a well known MOF, where Cu-based metal-oxygen SBUs are connected by trimesic acid linkers. Each linker features three carboxylic groups in a triangular arrangement and binds to three copper clusters. We

assume that this linker maintains a rigid planar configuration, defined by three carbon atoms of COO groups attached to the SBUs. In the molecular truss, the triangular shape of the linker requires an additional site (we use a carbon site here for the convenience of terminology) in the centre of the truss, bonded to the neighboring sites as shown in Fig. S3. The network of bonds ensures that the whole structure is planar. It can be seen as composed of four rigid flat tetrahedra (or pyramids). Three of these tetrahedra are formed by two carbon sites and two oxygen sites each (shown in yellow) and one tetrahedron is formed by four carbon sites (shown in purple in S2). The yellow tetrahedra retain independent rotational freedom along the axis connecting the carbon site attached to the oxygen sites and the site in the center of the truss. The attachment to the SBU, where two oxygen sites are shared between the SBU and the linker, again corresponds to a hinge connection.
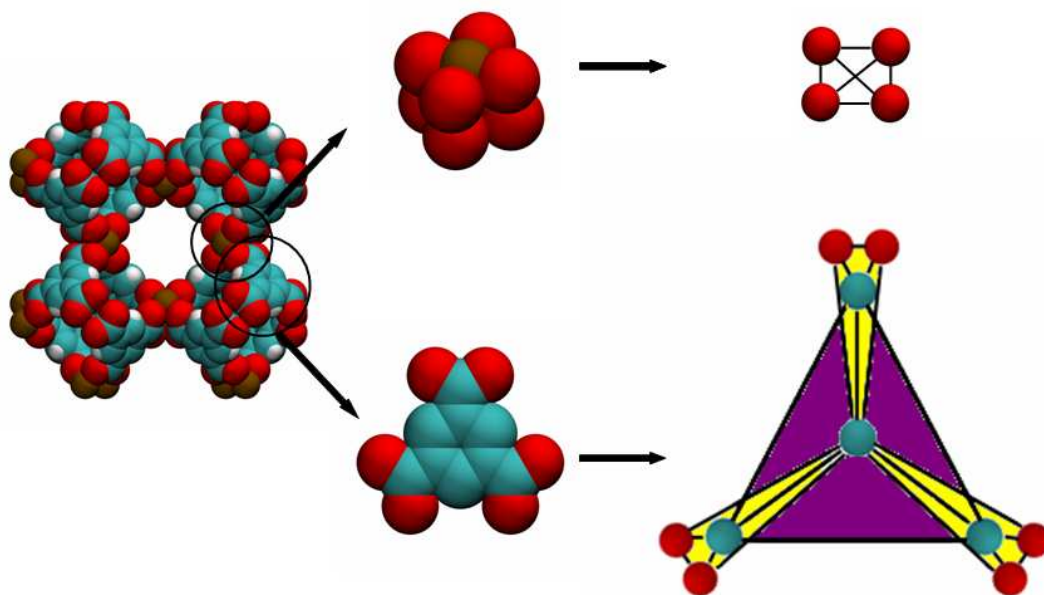

Fig. S3: Construction of a molecular truss representation of HKUST-1. The metal-oxygen SBU on the top is reduced to a system of oxygen sites, connected by rigid bonds (top). The trimesic acid linker becomes a molecular truss of ten sites as shown in the lower part of the figure. Color scheme for the molecular visualization of HKUST-1 on the left: cyan for carbon, red for oxygen, brown for copper, white for hydrogen.

Section S2. Visualization of molecular trusses

For better visualization of molecular trusses in the main text of the article and in the supplementary video files, we adopt an approach where all the individual trusses, formed by the groups of three bonded sites, are colored red in the SBUs and light blue in the linkers. Fig. S4 shows an example of this visualization for IRMOF-1.
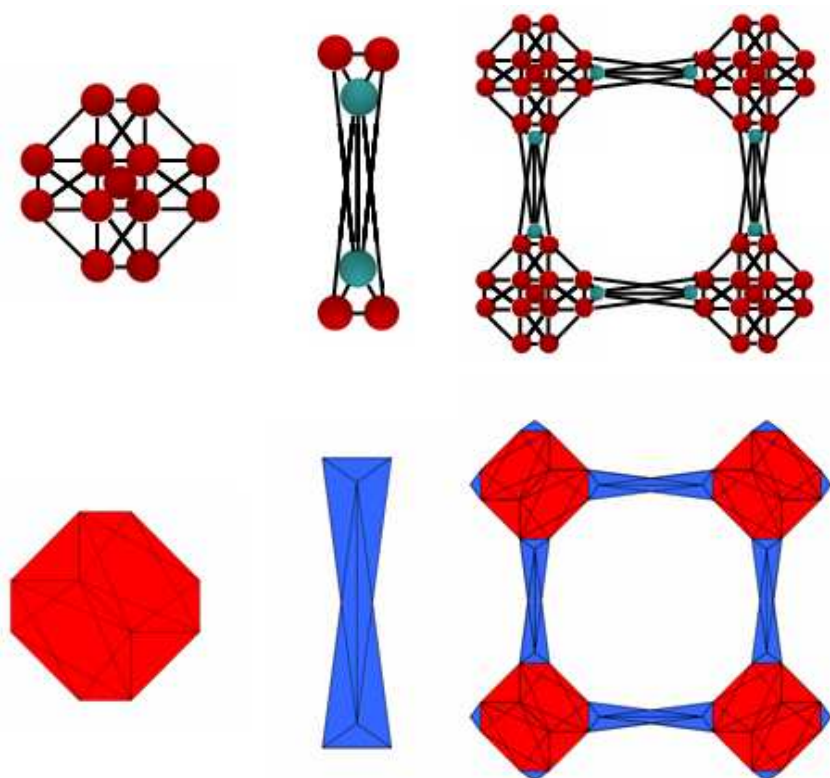

Fig. S4. Schematic illustration of the actual molecular trusses in IRMOF-1 (top row, not all bonds are shown in the SBU for clarity) and the adopted visualization scheme for these trusses in the main article and in the supplemented video materials (bottom row).

Section S3. Mechanical models

Mechanical models were constructed using basic building materials: solid wood pieces, veneer sheets, 3/4 in. brass hinges, blue and red paint, and superglue.
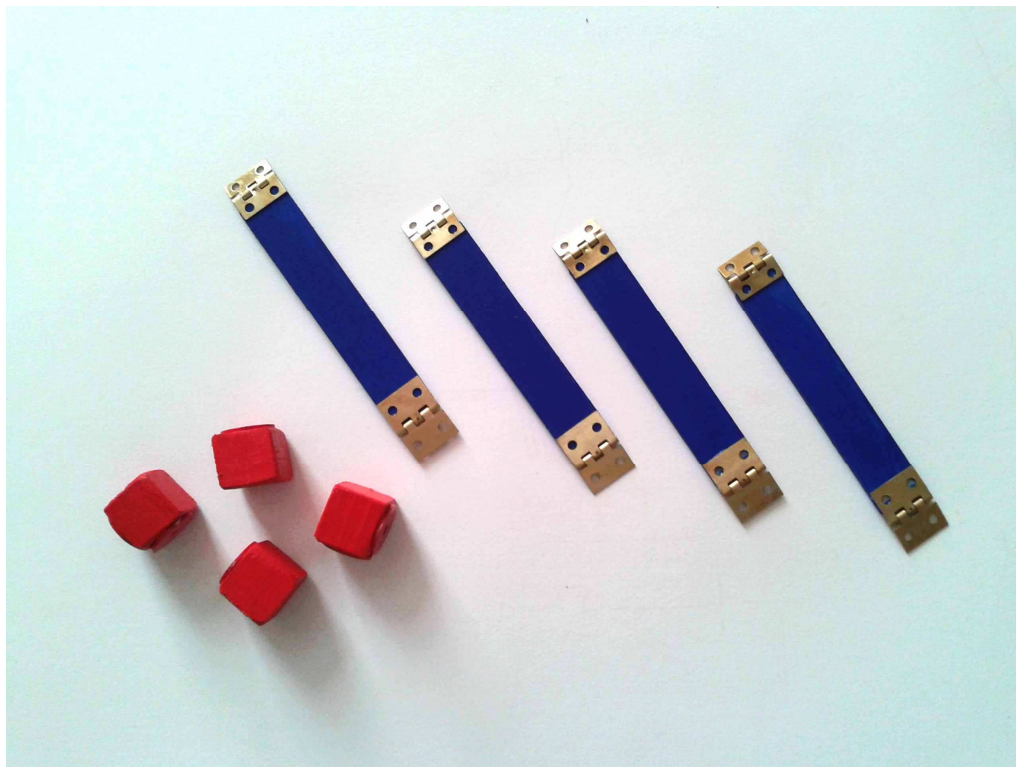

Fig. S5. The mechanical model building blocks: red cubes represent SBUs, blue bars correspond to linkers, with the hinges shown glued to the blue bars.

A supplementary video material explaining the construction process and the flexibility regimes in the mechanical models is provided at:
http://www.nanoporousmaterials.org/flexibility/

Section S4. Mechanical models for IRMOF-1 fragments, MIL-53 and HKUST-1

Fig. S6 below shows the mechanical toy model for a single face of IRMOF-1. The model is not flexible if constrained to a motion in plane (2D), by for example placing it on the table. In 3D the model can flex in a number of ways as shown in the figure.
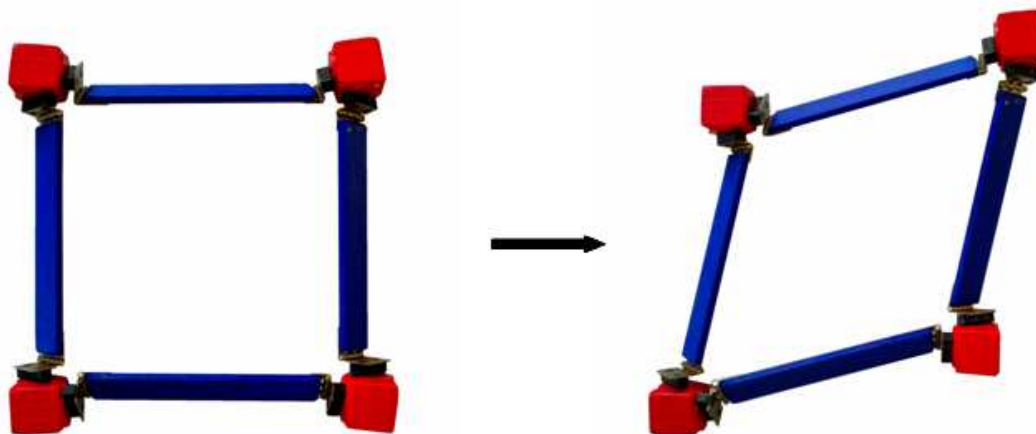

Fig. S6: A simple mechanical model of a single face of IRMOF-1, where red cubes are connected by blue rods via hinges at 45° angle to the plane of the figure, demonstrates that this structure is very flexible in three dimensions.

From the molecular visualization of MIL-53, one can view this structure as long clusters or chains formed by metal and oxygen atoms (Fig. S7). The rigid carboxylic linkers are attached to these chains via hinges, with all of them oriented parallel to each other. A mechanical model of this structure is shown in Fig. S7 (with metal-oxygen clusters shown as red, parallel rods, and linkers as blue rods). Parallel orientation of the hinges allows concerted movement of all linkers in the same plane and this results in a high level of structural flexibility as shown in Fig. S7.

Fig. S8 shows the mechanical model for HKUST-1, where trimesic acid linkers are represented by solid triangular elements (blue). Here we note that this structure is mechanically rigid.

Several videos of flexible and rigid mechanical models of MOFs are provided at:
http://www.nanoporousmaterials.org/flexibility/
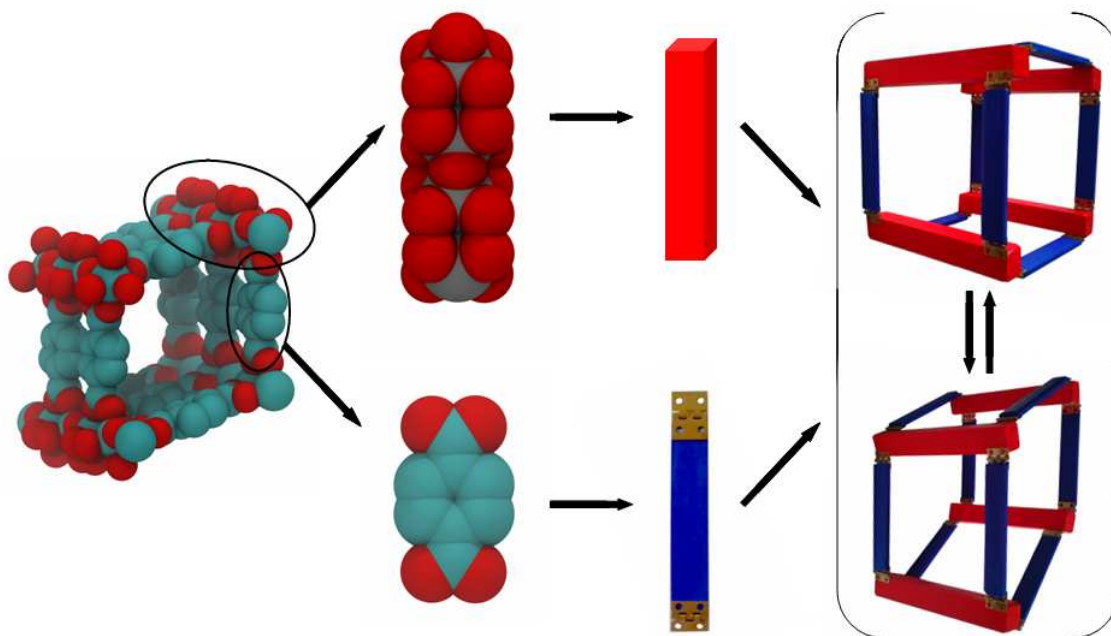
Fig. S7: Mechanical model of MIL-53. Flexible mechanical modes of the structure are shown on the right.
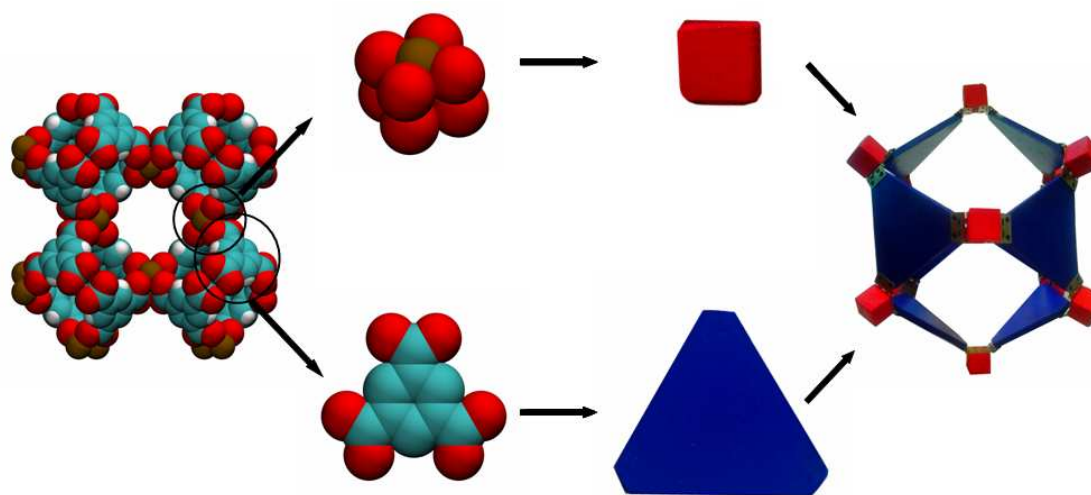
Fig. S8. Mechanical model of HKUST-1.

Section S5. Analysis of flexible modes in the systems of molecular trusses

Our representation of a MOF as a system of molecular trusses preserves periodic boundary conditions. Links between the sites are described as stiff harmonic springs. The unit cell of the molecular truss is perturbed according to one or a combination of the modes schematically depicted in Fig. S9. This perturbation is described by the order parameter, d, which characterizes the deviation of the lattice parameter of the unit cell from the original value. For example, for a unit cell with lattice parameters $a, b, c, \alpha, \beta, \gamma$ (using standard notation), compression or expansion along vector a, can be described as:

$$a* = da \qquad (1)$$

where a is the original length of the unit cell along the a vector, and $a*$ is the new value of a as a result of compression or expansion by factor d. Similarly, linear compression or expansion corresponds to simultaneous application of the following deformations:

$$a* = da$$
$$b* = db \qquad (2)$$
$$c* = dc$$

while shear deformation (in xy plane) corresponds to

$$\gamma* = d\gamma \qquad (3)$$

Steepest descent energy minimization method is used to find the conformation of the structure within the deformed unit cell, with the energy formulated as:

$$E = \frac{k\sum_{ij}(c_{ij} - c_{ij}^0)^2}{N} \qquad (4)$$

where E is the energy of the system per bond, c_{ij} is the current distance between sites i and j,

c_{ij}^0 is the equilibrium distance between sites i and j, corresponding to the initial input crystal

structure, N is the number of bonds in the system, k is an arbitrary constant and summation

takes place over all bonds in the system. A flexible structure, compatible with a particular

deformation, should exhibit very little penalty (within a numerical error) upon energy

minimization. On the other hand, a graph, incompatible with a particular geometry of the unit

cell, will be able to adapt to this geometry only via substantial expansion or contraction of the

links, and hence a large energy penalty.

Linear compressibility   Young modulus

Shear modulus   Poisson ratio
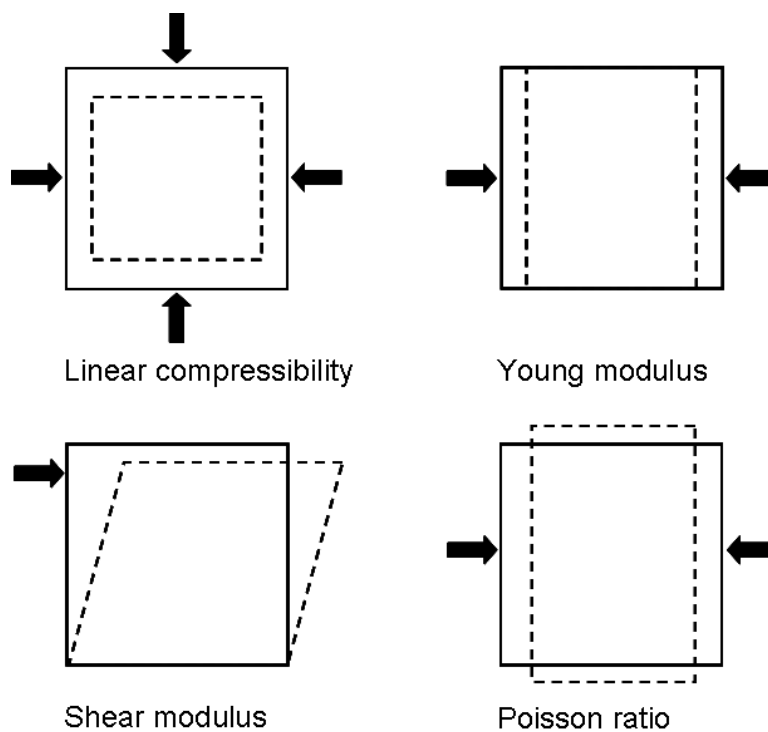
Fig. S9: Several classes of crystal structure deformations and the elastic properties

associated with them.

What is also important to remember is that the perturbations of the unit cell described above

should be sufficiently small to avoid unrealistic, artifact deformations arising from the sites

having no size and the bonds being able to cross each other. An example of this behavior is

shown in Fig. S10, for IRMOF-1, undergoing isotropic compression-expansion of a and b

lattice vectors with simultaneous relaxation of the system in *c*. As can be seen from the figure, the initial response of the structure in a range of small perturbations (0.98<*d*<1.016) is parabolic, and remains so upon further expansion (*d*=1.020). However, when compressed beyond *d*=0.98, the behavior of the energy penalty shows a different pattern associated with a series of collapsed, unphysical structures (as can be confirmed by visual inspection of the conformations). Within our analysis, this behavior is qualified as rigid, since the only way the system can accommodate this deformation is via substantial energy penalty and collapse.
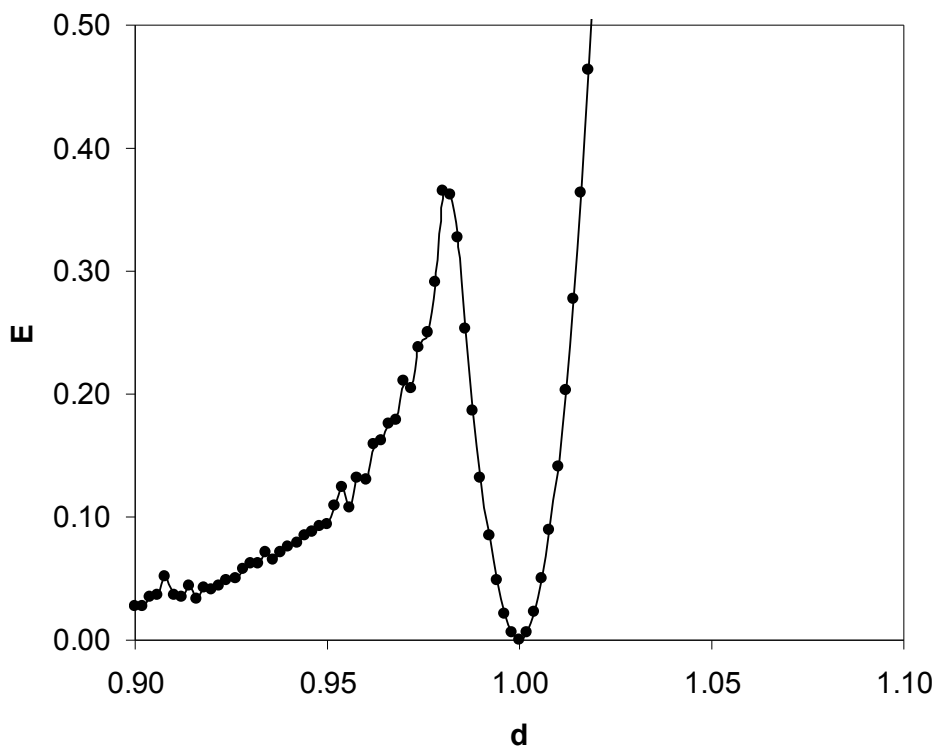

Fig. S10: Energy penalty as a function of order parameter for IRMOF-1 under isotropic compression-expansion of *a* and *b* lattice vectors with simultaneous relaxation of the system in *c*.

Below we provide examples of flexible and rigid regimes in MIL-53 (Figure S11).
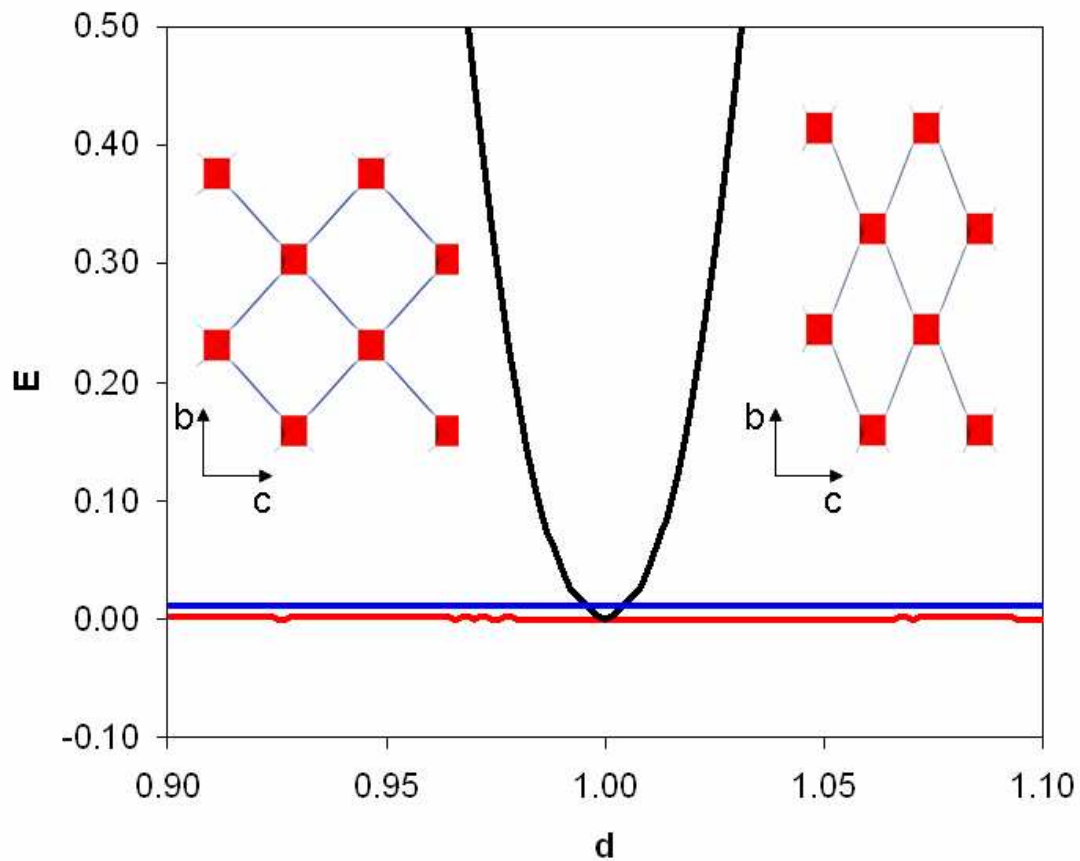
Figure S11. Energy penalty as a function of order parameter (degree of perturbation) for MIL-53. Black line corresponds to perturbation of α unit cell angle (shear deformation); red line corresponds to compression-expansion of lattice vector b, with simultaneous relaxation of lattice vector c. Blue line corresponds to the threshold value of the energy penalty (E=0.01). If the energy penalty is below this value for all values of the order parameter, the structure is classified as flexible with respect to this deformation. Snapshots on the left and right illustrate the geometry of the system, corresponding to the points on the red line (d=0.94 and d=1.10). In these snapshots, red molecular trusses represent metal-oxygen chains, connected by blue molecular trusses, corresponding to linkers.

As seen from Figure S11, MIL-53 shows rigid behavior with respect to the perturbation of α unit cell angle (shear deformation). However, when compressed (or expanded) along b lattice vector with simultaneous relaxation of lattice vector c, MIL-53 experiences essentially zero

energy penalty, as shown by red line in Figure S11. In practice, energy penalty E, as defined by Equation 4, is never exactly zero due to small deviations of bonds from their equilibrium length values and round-off errors; this function is always positive. Using insights from the results on MIL-53, we define a threshold value of E=0.01, below which the energy penalty is considered to be effectively zero. This threshold is shown as blue line in Figure S11.

Each material has been investigated using total of thirteen perturbation regimes, with these regimes summarized in Table S1.

Table S1. Perturbation of one or more lattice parameters gives a unique perturbation regime. Dot (●) corresponds to the lattice parameter being perturbed, dash (-) to the lattice parameter being fixed, and square (■) corresponds to a lattice parameter allowed to relax, as a response to the perturbation of other lattice parameters.

Perturbation\Cell parameter	a	b	c	α	β	Γ
ABC	●	●	●	-	-	-
A (Young)	●	-	-	-	-	-
B (Young)	-	●	-	-	-	-
C (Young)	-	-	●	-	-	-
Alpha (Shear)	-	-	-	●	-	-
Beta (Shear)	-	-	-	-	●	-
Gamma (Shear)	-	-	-	-	-	●
AB (Poisson)	●	■	-	-	-	-
AC (Poisson)	●	-	■	-	-	-
BC (Poisson)	-	●	■	-	-	-
AB-C	●	●	■	-	-	-
AC-B	●	■	●	-	-	-

BC-A	■	●	●	-	-	-

We recognize two main classes of behavior as a result of one of the perturbations summarized in Table S1. They are:

.

1) A MOF is considered to be flexible with respect to a particular deformation, if the energy penalty is zero (E<0.01) for all values of the order parameter. Red line in Figure S11 is an example of this behavior.

2) A MOF is considered to be rigid with respect to a particular deformation, if the energy penalty is above zero (E>0.01) for any values of the order parameter. Figure S10 and black line in Figure S11 are examples of this behavior.

For the vast majority of cases, these simple criteria are sufficient to classify MOFs into flexible and rigid structures. However, a small fraction of tests (20 out of 299 explored, or less than 7%) exhibit behavior which we would like to group into a separate category. In this category two scenarios are possible:

1) The energy penalty is continuously zero (E<0.01), but only on a limited interval of the order parameter. An example of this behavior is shown below for shear deformation of the **pcu** material (see Section S7 for the summary of materials explored):
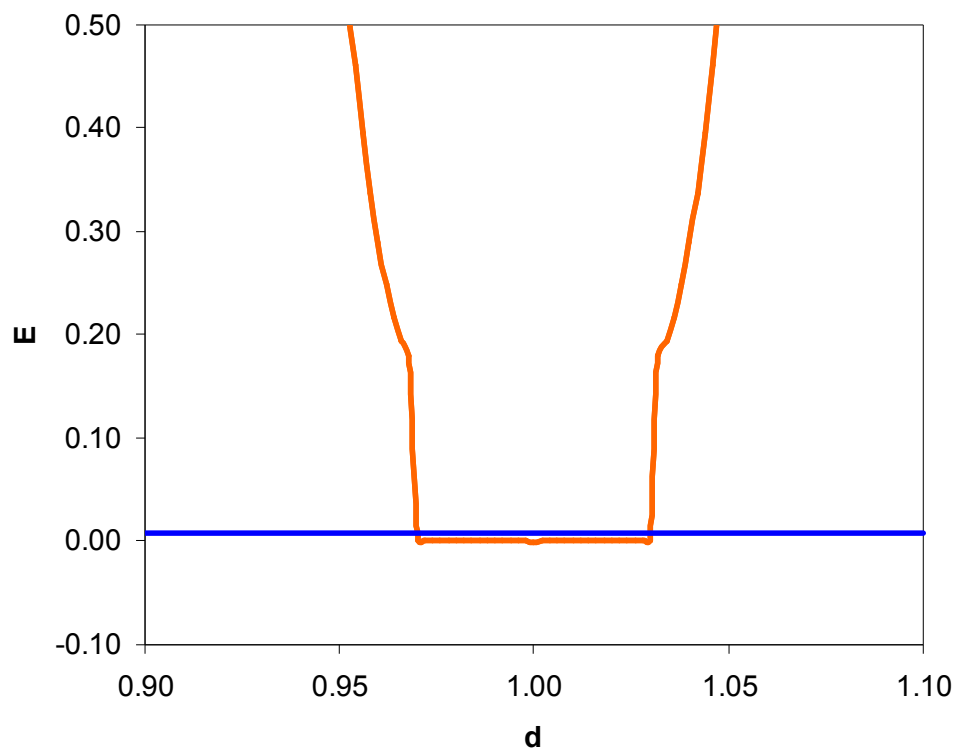
Figure S12. Energy penalty as a function of order parameter (degree of perturbation) for the **pcu** material (see Section S7). Orange line corresponds to perturbation of α unit cell angle (shear deformation); blue line corresponds to the threshold value of the energy penalty (E=0.01).

2) Energy penalty remains continuously low for all values of the order parameter, but exceeds the threshold value (E=0.01). In fact only one material (MIL-88) showed this type of behavior. This behavior is shown below in Figure S13:
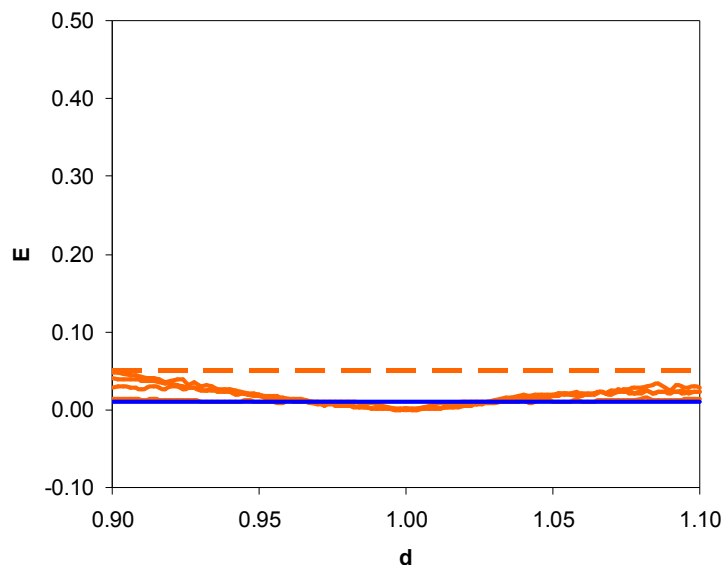
Figure S13. Energy penalty as a function of order parameter (degree of perturbation) for MIL-88 material. Orange lines correspond to B, Alpha, AB, AC, BC perturbations as defined in Table S1. Blue line corresponds to the threshold value of the energy penalty (E=0.01). Dashed orange line corresponds to the additional threshold value of the energy penalty (E'=0.05)

We use an additional threshold value of the energy penalty (E'=0.05) to define this behavior. We define modes following either of the two special scenarios described above as semi-flexible modes. Occasional appearance of these modes has almost no effect on classification of materials into rigid and flexible structures, as structures featuring semi-flexible modes, would usually also feature properly flexible modes. Only 2 materials out of 23 exhibited exclusively semi-flexible modes.

In section S9 we summarize energy graphs for ALL tests and for the vast majority of the cases classification of the MOF behavior into rigid or flexible is quite simple and unambiguous and does not require any special considerations.

Here it is important to emphasize that the proposed method is meant to serve as a pre-screening tool in order to identify *potential* modes of flexibility to be further investigated using more rigorous molecular modeling or experimental methods.

Figure S14 below compares swelling behavior in MIL-88 as predicted by the mechanical models and from the experimental results of Mellot-Draznieks *et al*[1].
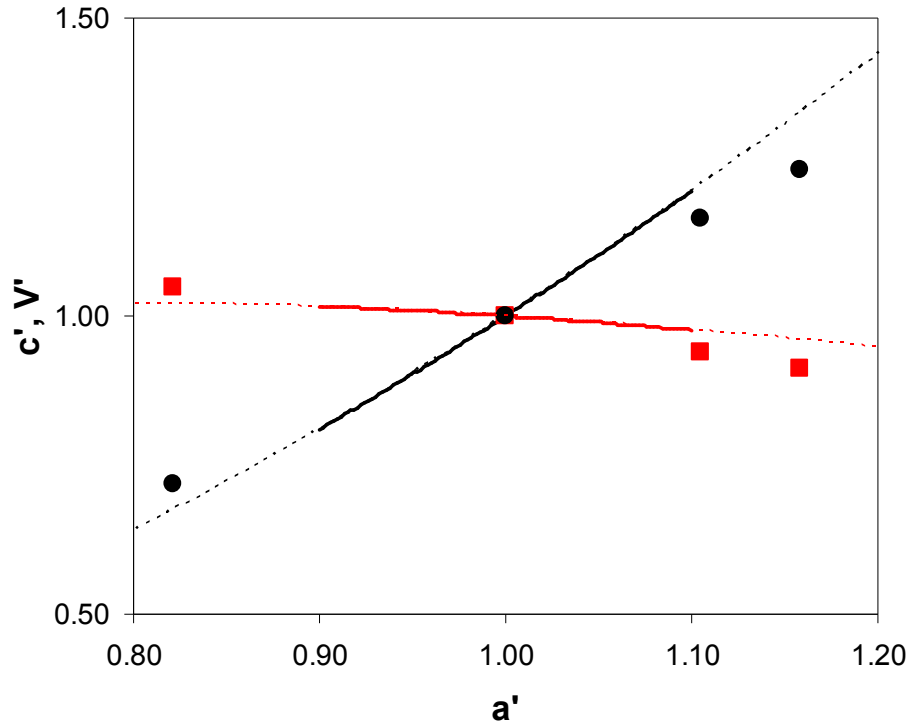

Figure S14. Lattice parameters of MIL-88 and swelling effects. Behavior of the normalized lattice vector *c'* (red lines and symbols) and volume *V'* (back lines and symbols) of the unit cell of MIL-88 as a function of the normalized vector *a'*. Solid lines are results from our approach, and symbols are results from experiments on MIL-88A[1]. Dashed lines extrapolate simulated behavior beyond the sampled region.

Section S6. Generation of hypothetical MOFs within RCSR topological classes

Despite a very large number of possibilities, it has been observed that the synthesis of three-dimensional frameworks comprising building blocks of particular shape overwhelmingly favors high symmetry topological arrangements[2]. Accordingly, it has been suggested that the highest symmetry three-dimensional topologies (or *nets*) are the most feasible targets for design of frameworks, so long as building blocks of the appropriate shape can be identified[3].

Therefore, we have chosen to explore all the *regular*, *semiregular*, *minimal* and *edge-transitive binodal* nets described in Ref. *3* for which we could identify previously synthesized and charge-balanced metal SBUs of the appropriate connectivity[4]. The nets explored are given in Table S5, and the corresponding organic and metallic building units are listed therein.

For each net, we computationally assembled metal-organic framework structure models exhibiting the required topology (i.e. hypothetical or *H*MOFs). This was achieved by attaching rigid building blocks together following the crystallographic description of each net provided at the Reticular Chemistry Structural Resource (http://rcsr.anu.edu.au).

Section S7. Summary of the investigated materials

Table S2: Summary of organic linkers in MOFs considered in this work

Name	Formula	Chemical structure
Benzene-1,4-dicarboxylic acid (BDC)	C_6H_4-1,4-$(CO_2H)_2$	
Benzene-1,3,5-tricarboxylic acid (BTC)	C_6H_3-1,3,5-$(CO_2H)_3$	
Benzene-1,2,3,4,5,6-hexacarboxylic acid (BHC)	C_6-1,2,3,4,5,6-$(CO_2H)_6$	
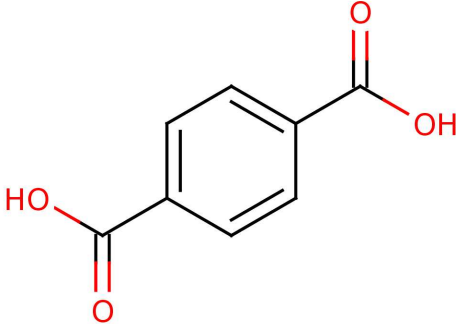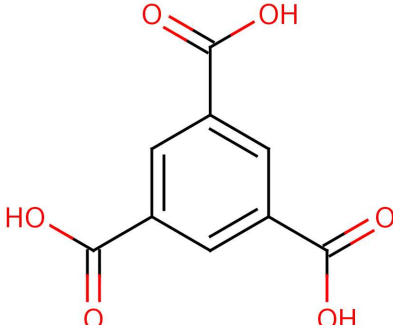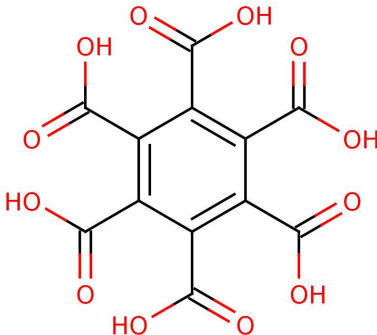
|		
2,6-naphthalenedicarboxylic acid (NDC)	$C_{10}H_6$-$(CO_2H)_2$	
2,5-dihydroxybenzenedicarboxylate (DHBDC)	C_6H_2-1,4-$(CO_2H)_2$-2,5-$(OH)_2$	
4,4',4''-(benzene-1,3,5-triyl-tris(ethyne-2,1-diyl))tribenzoate (BTE)	C_6H_3-$((C_2)(C_6H_4)(CO_2H))_3$	
Methanetetrabenzoate (MTB)	C-$((C_6H_4)(CO_2H))_4$	
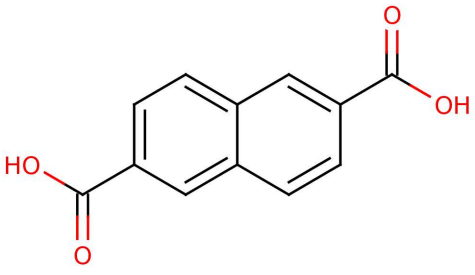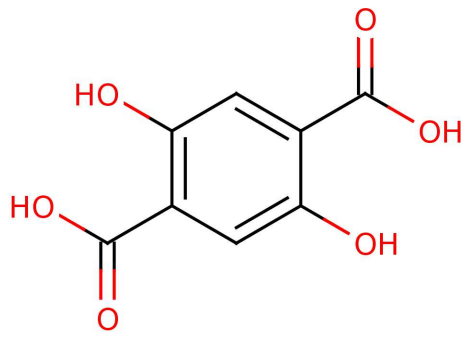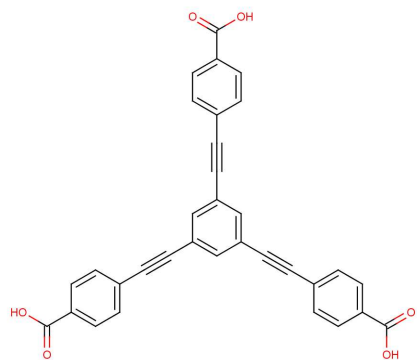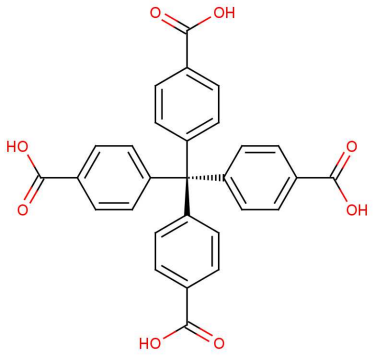
1,3,5-tris[((1,3-carboxylic acid-5-(4-(ethynyl)phenyl)) ethynyl)phenyl]-benzene (LH$_6$)	C$_6$H$_3$-(C$_6$H$_4$-C$_2$-C$_6$H$_4$-C$_2$-(C$_6$H$_4$-(CO$_2$H)$_2$))$_3$	
1,4-diazabicyclo[2.2.2]octane (DABCO)	N-(C$_2$H$_4$)$_3$-N	
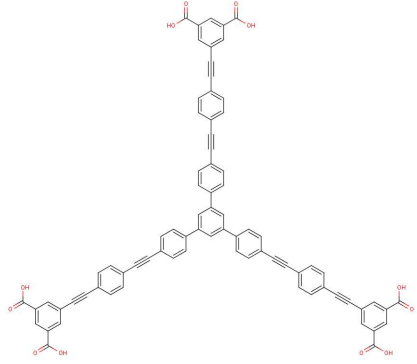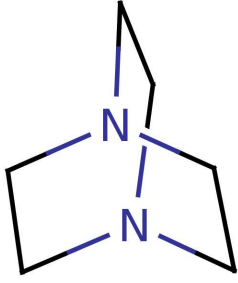
Table S3: Summary of metal-oxygen SBU clusters and rods in MOFs considered in this work

Formula	Connectivity
Cu$_2$	Square
Zn$_2$	Square
Zn$_4$O	Octahedral
V$_4$(OH)$_4$	Tetrahedral
Ti$_6$O$_6$	Hexagonal
Pd$_3$	Trigonal prismatic
(VO)$_n$	Helical rods, square
(CrO)$_n$	Helical rods, square
Fe$_3$O	Trigonal prismatic
(ZnO)$_n$	Helical rods, trigonal

Table S4. Summary of investigated experimental MOFs

Name	Net	SBU/Chain	Linker	Ref
IRMOF-1	**pcu**	Zn$_4$O	BDC	(5)
MIL-47	**sra***	(VO)$_n$	BDC	(6)
MIL-53	**sra***	(CrO)$_n$	BDC	(7)

MIL-88	**acs**	Fe_3O	NDC	(*8*)
HKUST-1	**tbo**	Cu_2	BTC	(*9*)
MOF-180	**qom**	Zn_4O	BTE	(*10*)
MOF-74	**bnn***	$(ZnO)_n$	DHBDC	(*11*)
MOF-36	**pts**	Zn_2	MTB	(*12*)
NU-110	**ntt** (or **rht**)	Cu_2	LH_6	(*13*)
DYB$^+$	**pcu**	Zn_2	BDC, DABCO	(*14*)

*Identification of the underlying nets of crystal structures, in particular the special case of those comprising infinite, rod-like metal SBUs is discussed in detail in Ref. *15*.

$^+$For convenience of reference we call the MOF reported by Dybtsev *et al.*[14] DYB.

Table S5. Summary of investigated hypothetical MOFs*

Name; net	SBU	Linker
acs	Pd_3	BDC
bor	$V_4(OH)_4$	BTC
cds	Cu_2	BDC
dia	$V_4(OH)_4$	BDC
hxg	Ti_6O_6	BDC
lvt	Cu_2	BDC
nbo	Cu_2	BDC
pcu	Zn_4O	BDC
pto	Cu_2	BTC
pyr	Zn_4O	BTC
rhr	Cu_2	BDC
she	Cu_2	BHC
sod	$V_4(OH)_4$	BDC

*All nets described in Ref. *2* and available from the Reticular Chemistry Structural Resource (http://rcsr.anu.edu.au).

Visualization of all MOFs including their molecular truss representation is provided at:

http://www.nanoporousmaterials.org/flexibility/

Section S8. Analysis of flexibility of 50 hypothetical MOFs from the database by Wilmer et al.[16]

In this section we provide additional details of the flexibility analysis of the hypothetical MOFs from the database of Wilmer et al.[16]. It is convenient to start this section with an experimental structure reported by Dybtsev et al.[14] (we label it DYB here). This MOF is based on two types of linkers. Paddle-wheel metal-oxygen clusters are bridged by carboxylate linkers (BDC in the work of Dybtsev and co-workers) to form 2D layers, with these layers extended into a 3D structure by pillars, based on nitrogen coordinating with the metal of the paddle-wheel (via dabco linker in the work of Dybtsev and co-workers). This results in a topology with a parallel orientation of all the hinges of the carboxylic groups along the channels of the structure, and this is responsible for the shape-shifting behavior of the material upon applied stimuli (inclusion of benzene molecules in the structure as reported in the original work).

In our model of DYB we did not consider any flexibility associated with the dabco linker and treated its connection to the paddle-wheel cluster as rigid by imposing an appropriate system of molecular trusses. For other linkers or systems this condition may have to be reconsidered; however we note that alternative representations would result in further increased potential for flexibility. Within the current model DYB showed flexibility with respect to shear by changing the γ angle of the unit cell (the energy profile was not as flat as for other MOFs, classified as flexible. We attribute this to the way we treat the dabco linker; see visualizations at http://www.nanoporousmaterials.org/flexibility/). Visual inspection of the structures within the detected semi-flexible behavior revealed no collapsed or unphysical configurations, and we therefore classified the structure as flexible. This behavior is in agreement with experiments.

The diversity of structures in the database of Wilmer et al. arises from the variation of organic linkers within a certain topology of MOF. However, from the mechanical point of view 43 out of top 50 hypothetical MOFs (ranked according to their performance for volumetric methane storage) can be considered as variants of the DYB material: although the linkers are different, the topology of the material and how the linkers are connected to the SBUs remain the same.

Within our approach, all these structures can be represented with one kind of molecular truss network, and according to our analysis they should be flexible.

Similarly, six more materials from the database follow the molecular truss network of MIL-53, and hence are flexible. Finally, the one remaining structure from the pool of 50 can be represented with the same molecular truss network as IRMOF-1 and therefore is rigid.

Section S9. Summary of the observed flexibility regimes

Table S6. Flexibility regimes in experimental (*E*MOFs) and hypothetical (*H*MOFs) MOFs. Red color signifies MOF being flexible with respect to a particular regime, yellow color corresponds to a semi-flexible regime (either within narrow range of the order parameter, or not conforming to any of the expected behavior and requiring further investigation).

*E*MOFs	ABC	A	B	C	Alpha	Beta	Gamma	AB	AC	BC	AB-C	AC-B	BC-A
IRMOF-1													
HKUST-1													
MIL-47										red			
MIL-53										red			
MIL-88			yellow		yellow			yellow	yellow	yellow	red		
MOF-180													
MOF-74													
MOF-36													
NU-110													
DYB							red						
*H*MOFs	ABC	A	B	C	Alpha	Beta	Gamma	AB	AC	BC	AB-C	AC-B	BC-A
acs											red		
bor													
cds					red	red	red						
dia					yellow	yellow	yellow				red		
hxg													
lvt								red	red	red	red	red	red
nbo					red	red	red						
pcu					yellow	yellow	yellow						
pto					yellow	yellow	yellow	yellow	yellow	yellow	yellow	yellow	yellow
pyr													
rhr								red	red	red	red	red	red
she													
sod								red	red	red	red	red	red

The videos of different flexibility regimes in MOFs using molecular truss representation are provided at:

http://www.nanoporousmaterials.org/flexibility/

Below we show all graphs used for the material classification in Table S6. Red, orange and black lines in these graphs correspond to flexible, semi-flexible and rigid modes, respectively. Horizontal blue line shows the position of the zero energy threshold (E=0.01).

A. Flexible modes (E<0.01):

MIL-47: BC	MIL-53: BC
MIL-88: AB-C	**DYB: Gamma**
acs: AB-C	**cds: Alpha, Beta, Gamma**

dia: AB-C

lvt: AB, AC, BC, AB-C, AC-B, BC-A

rhr: AB, AC, BC, AB-C, AC-B, BC-A

sod: AB, AC, BC, AB-C, AC-B, BC-A
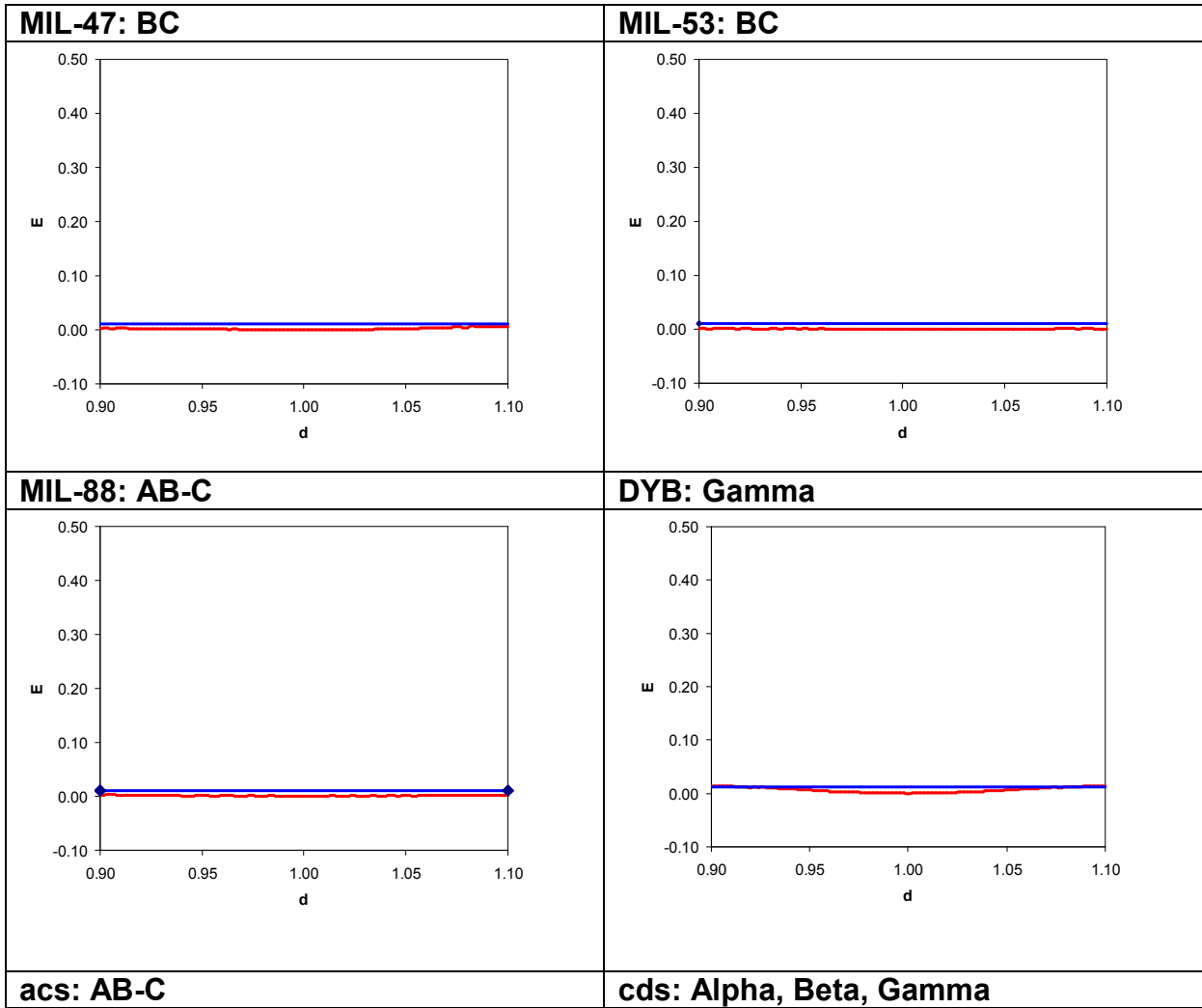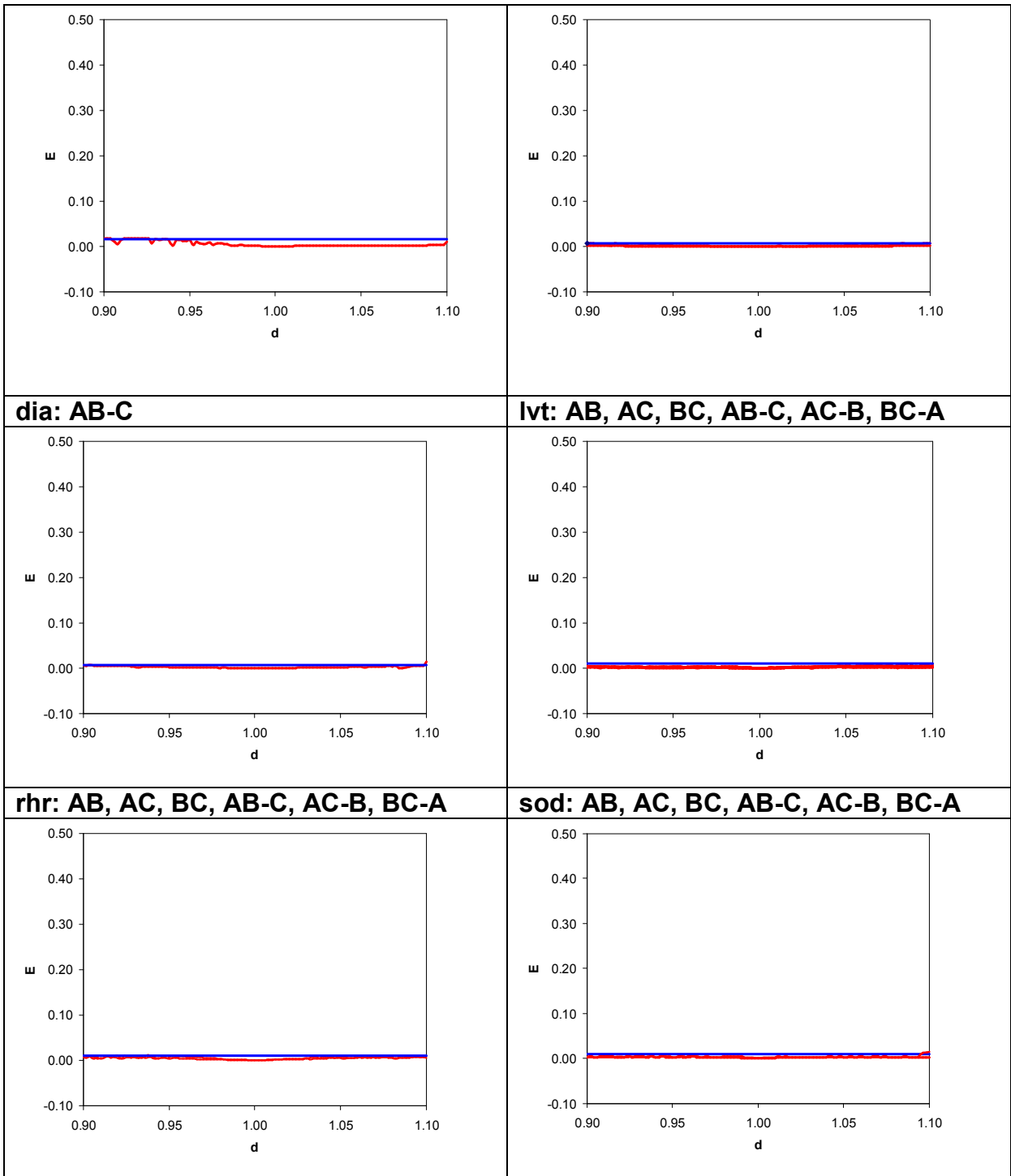
B. Semi-flexible modes:

pto: Alpha, Beta, Gamma, AB, AC, BC, AB-C, AC-B, BC-A	pcu: Alpha, Beta, Gamma

MIL-88: B, Alpha, AB, BC, AC

dia: Alpha, Beta, Gamma
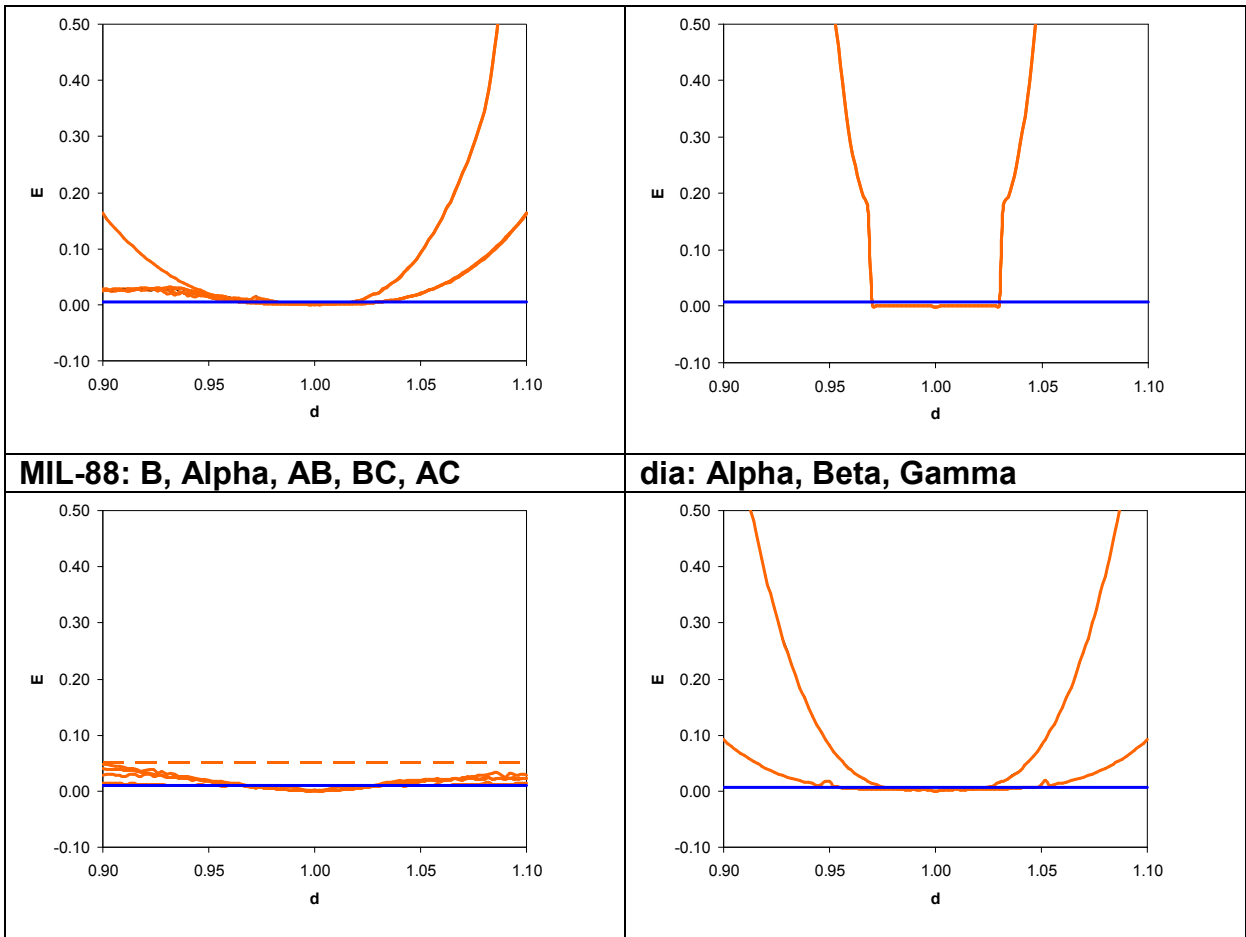


C. Rigid regimes (E>0.01): all remaining modes not listed in section A, B.

IRMOF-1

HKUST-1

MIL-47

MIL-53
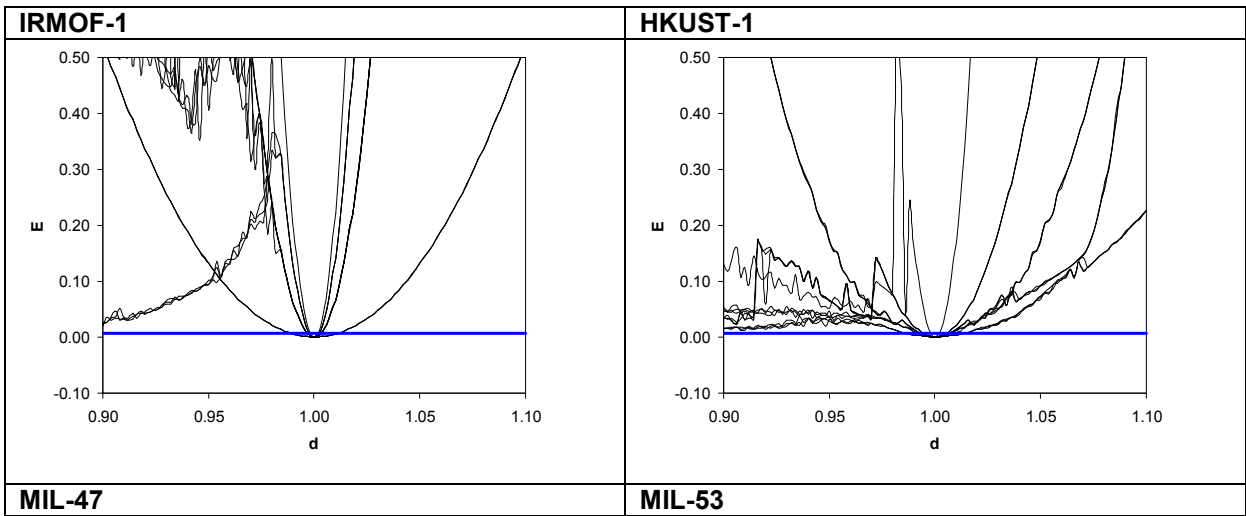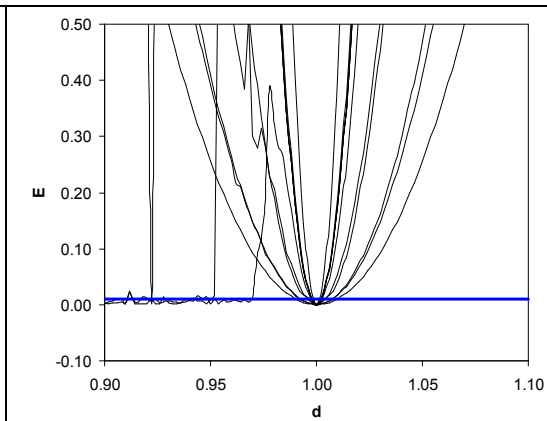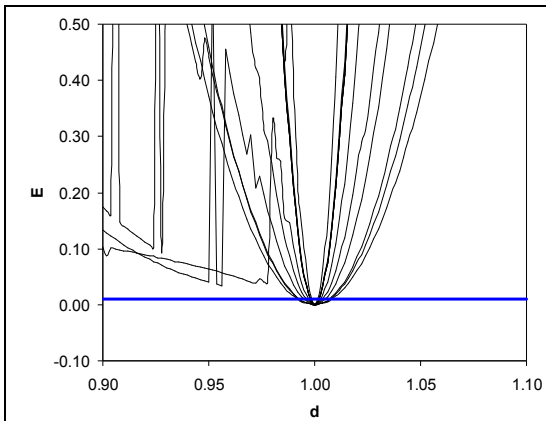
MIL-88

MOF-180
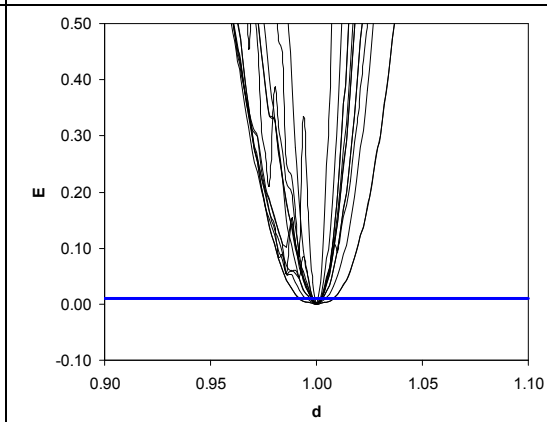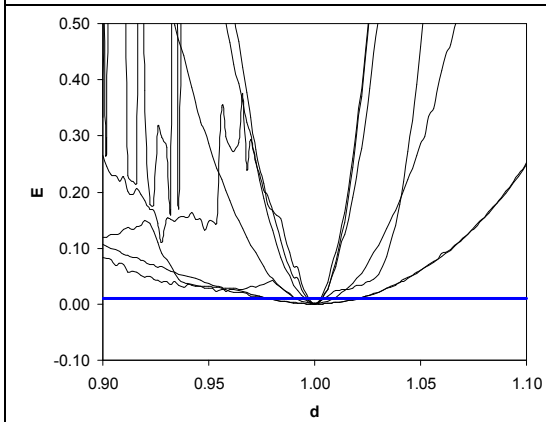
MOF-74

MOF-36
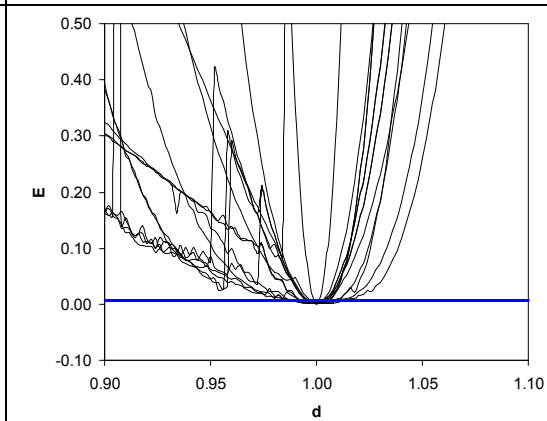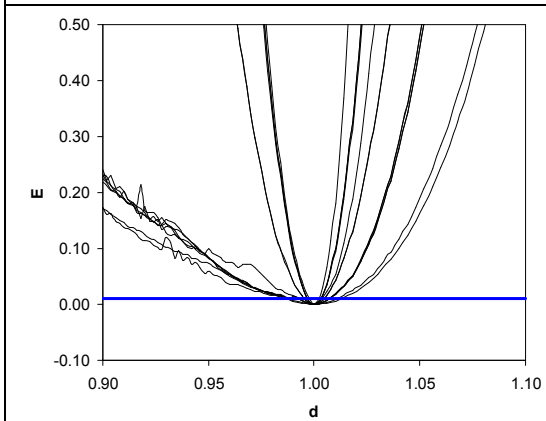
NU-110

DYB
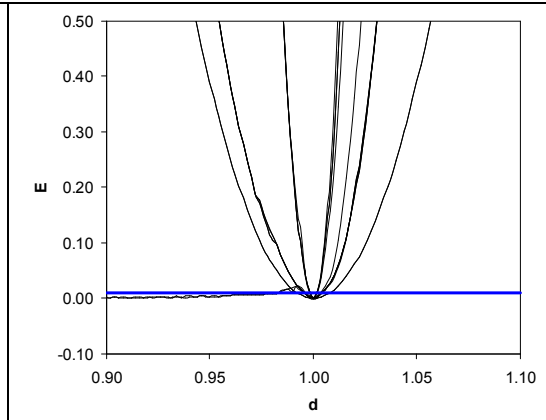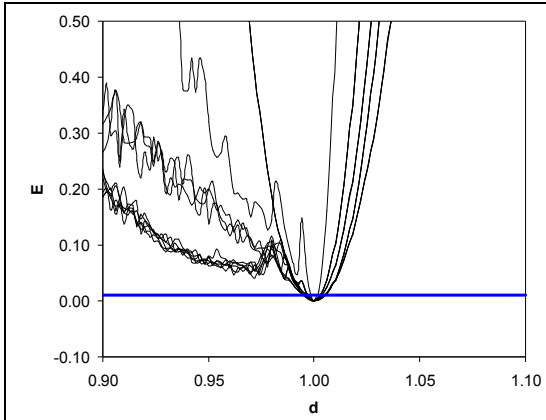
acs

bor

cds

dia

hxg

lvt

nbo

pcu

pto

pyr
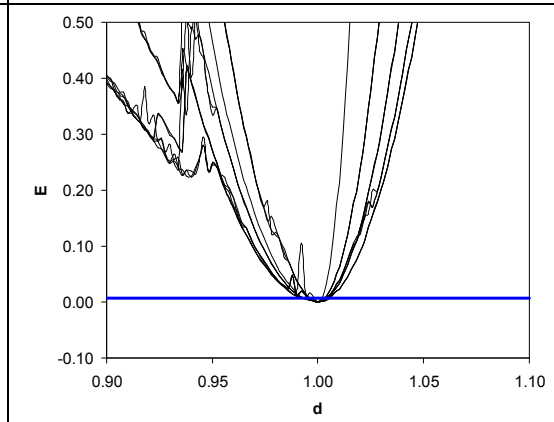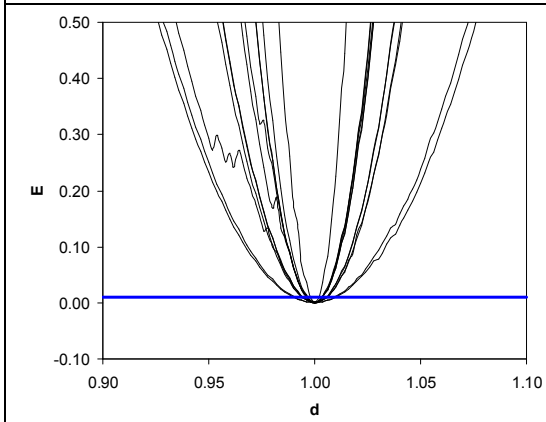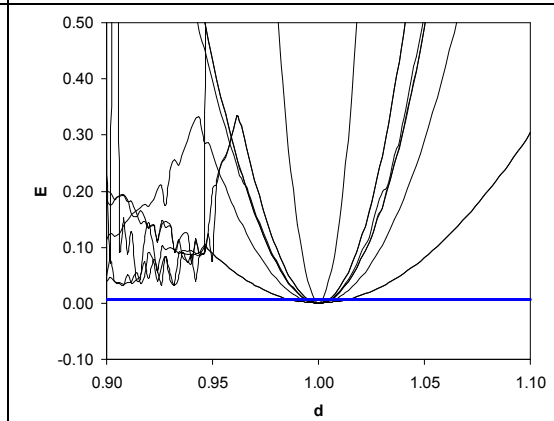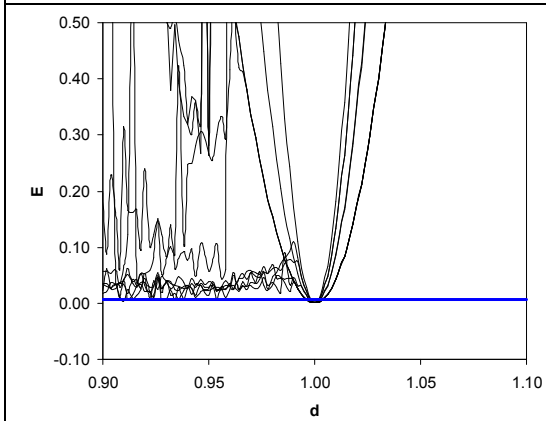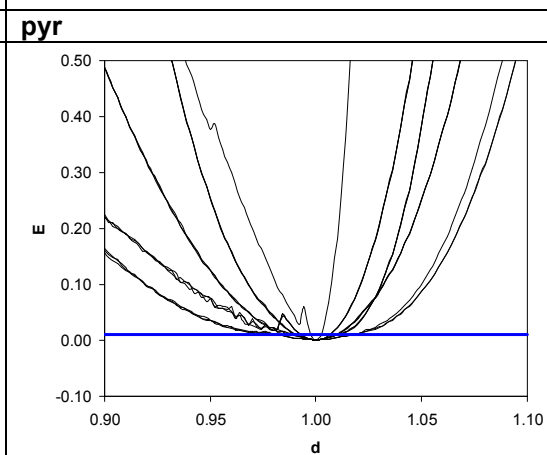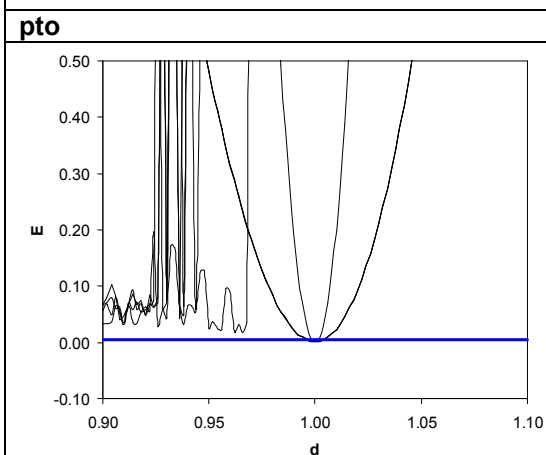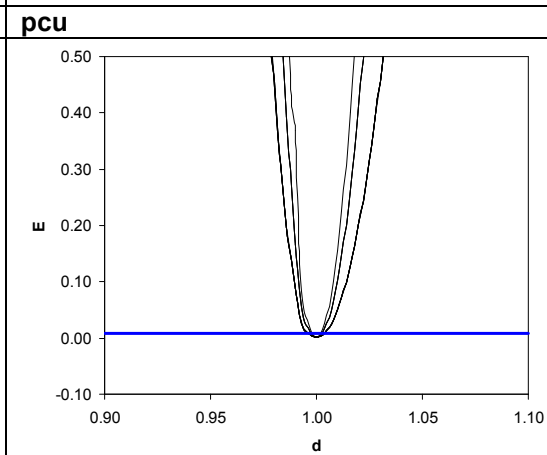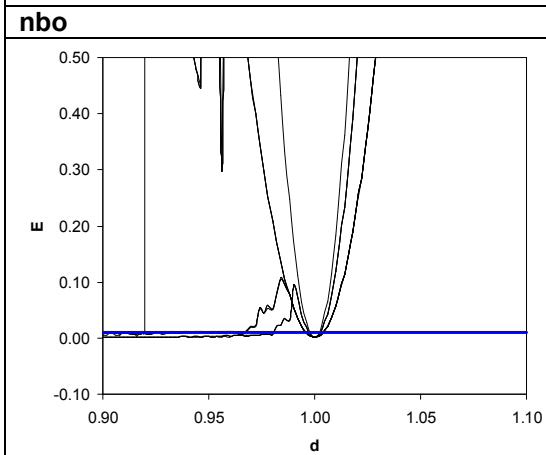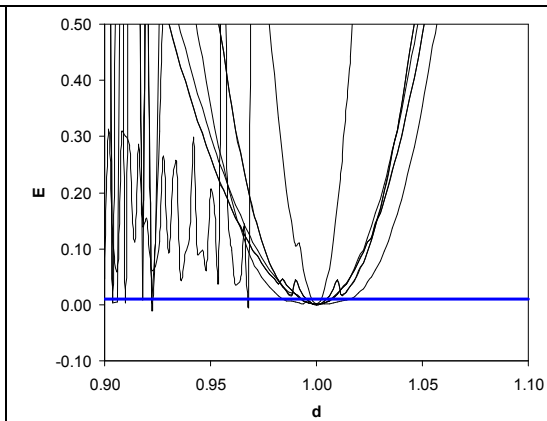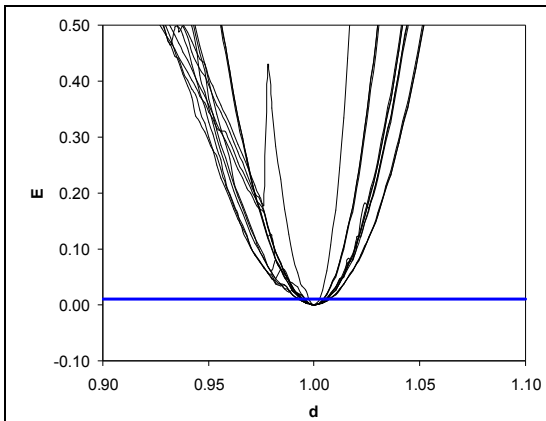
rhr

she
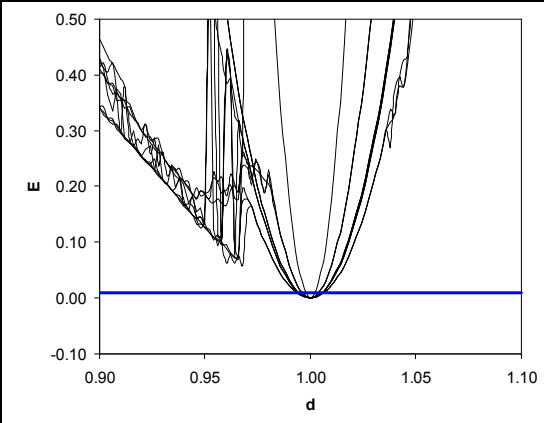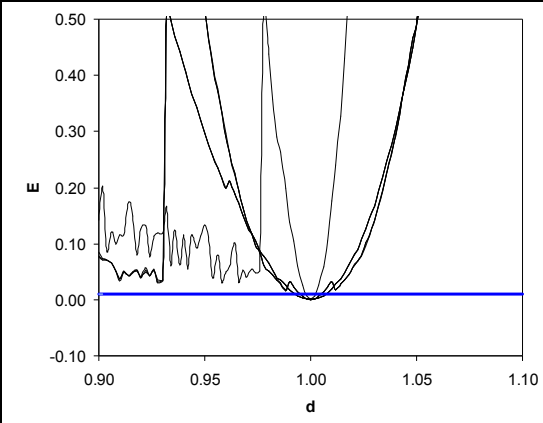
**sod**
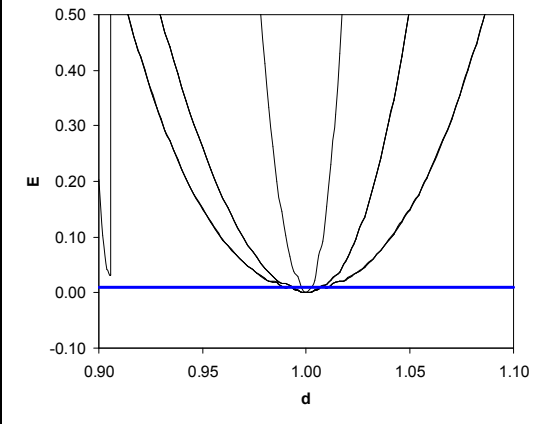
References

1. Mellot-Draznieks, C.; Serre, C.; Surble, S.; Audebrand, N.; Férey, G. Very large swelling in hybrid frameworks: A combined computational and powder diffraction study. *J. Am. Chem. Soc.* **127**, 16273-16278 (2005).

2. Ockwig, N.W., Delgado-Friedrichs, O., O'Keeffe, M. & Yaghi, O.M. Reticular chemistry: Occurrence and taxonomy of nets and grammar for the design of frameworks. *Acc. of Chem. Res.* **38**, 176-182 (2005).

3. Delgado-Friedrichs, O., O'Keeffe, M. & Yaghi, O.M. Taxonomy of periodic nets and the design of materials. *Phys. Chem. Chem. Phys.* **9**, 1035-1043 (2007).

4. Tranchemontagne, D.J., Mendoza-Cortes, J.L., O'Keeffe, M. & Yaghi, O.M. Secondary building units, nets and bonding in the chemistry of metal-organic frameworks. *Chem. Soc. Rev.* **38**, 1257-1283 (2009).

5. Li, H., Eddaoudi, M., O'Keeffe, M. & Yaghi, O.M. Design and synthesis of an exceptionally stable and highly porous metal-organic framework. *Nature* **402**, 276-279 (1999).

6. Barthelet, K., Marrot, J., Riou, D. & Férey, G. A breathing hybrid organic-inorganic solid with very large pores and high magnetic characteristics. *Angew. Chem. Int. Ed.* **41**, 281 (2002).

7. Serre, C. et al. Very large breathing effect in the first nanoporous chromium(III)-based solids: MIL-53 or Cr-III(OH)·{O2C-C6H4-CO2}·{HO2C-C6H4-CO2H}$_x$·H2O$_y$. *J. Am. Chem. Soc.* **124**, 13519-13526 (2002).

8. Serre, C., Millange, F., Surblé, S. & Férey, G. A Route to the Synthesis of Trivalent Transition-Metal Porous Carboxylates with Trimeric Secondary Building Units. *Angew. Chem. Int. Ed.* **43**, 6285-6289 (2004).

9. Chui, S.S.Y., Lo, S.M.F., Charmant, J.P.H., Orpen, A.G. & Williams, I.D. A chemically functionalizable nanoporous material [Cu-3(TMA)(2)(H2O)(3)](n). *Science* **283**, 1148-1150 (1999).

10. Furukawa, H. et al. Ultrahigh Porosity in Metal-Organic Frameworks. *Science* **329**, 424-428 (2010).

11. Rosi, N.L. et al. Rod Packings and Metal-Organic Frameworks Constructed from Rod-Shaped Secondary Building Units. *J. Am. Chem. Soc.* **127**, 1504-1518 (2005).

12. Kim, J. et al. Assembly of Metal-Organic Frameworks from Large Organic and Inorganic Secondary Building Units: New Examples and Simplifying Principles for Complex Structures. *J. Am. Chem. Soc.* **123**, 8239-8247 (2001).

13. Farha, O.K. et al. Metal-Organic Framework Materials with Ultrahigh Surface Areas: Is the Sky the Limit? *J. Am. Chem. Soc.* **134**, 15016-15021 (2012).

14. Dybtsev, D.N., Chun, H. & Kim, K. Rigid and Flexible: A Highly Porous Metal–Organic Framework with Unusual Guest-Dependent Dynamic Behavior. *Angew. Chem. Int. Ed.* **43**, 5033-5036 (2004).

15. O'Keeffe, M. & Yaghi, O.M. Deconstructing the Crystal Structures of Metal-Organic Frameworks and Related Materials into Their Underlying Nets. *Chem. Rev.* **112**, 675-702 (2012).

16. Wilmer, C.E. et al. Large-scale screening of hypothetical metal-organic frameworks. *Nat. Chem.* **4**, 83-89 (2011).